Assessment of Nuclear Resonance Fluorescence for Spent Nuclear Fuel Assay

Brian J. Quiter* and Bernhard A. Ludewigt†
Lawrence Berkeley National Laboratory, Berkeley, CA 94720

Scott D. Ambers‡
University of California, Berkeley, Nuclear Engineering, Berkeley, CA 94720 and
Lawrence Berkeley National Laboratory, Berkeley, CA 94720

In nuclear resonance fluorescence (NRF) measurements, resonances are excited by an external photon beam leading to the emission of gamma rays with specific energies that are characteristic of the emitting isotope. NRF promises the unique capability of directly quantifying a specific isotope without the need for unfolding the combined responses of several fissile isotopes as is required in other measurement techniques. We have analyzed the potential of NRF as a non-destructive analysis technique for quantitative measurements of Pu isotopes in spent nuclear fuel (SNF). Given the low concentrations of ^{239}Pu in SNF and its small integrated NRF cross sections, the main challenge in achieving precise and accurate measurements lies in accruing sufficient counting statistics in a reasonable measurement time.

Using analytical modeling, and simulations with the radiation transport code MCNPX that has been experimentally tested recently, the backscatter and transmission methods were quantitatively studied for differing photon sources and radiation detector types. Resonant photon count rates and measurement times were estimated for a range of photon source and detection parameters, which were used to determine photon source and γ-ray detector requirements. The results indicate that systems based on a bremsstrahlung source and present detector technology are not practical for high-precision measurements of ^{239}Pu in SNF. Measurements that achieve the desired uncertainties within hour-long measurements will either require stronger resonances, which may be expressed by other Pu isotopes, or require quasi-monoenergetic photon sources with intensities that are approximately two orders of magnitude higher than those currently being designed or proposed.

This work is part of a larger effort sponsored by the Next Generation Safeguards Initiative to develop an integrated instrument, comprised of individual NDA techniques with complementary features, that is fully capable of determining Pu mass in spent fuel assemblies.

* bjquiter@lbl.gov
† Bernhard_Ludewigt@lbl.gov
‡ sambers@umich.edu

I. INTRODUCTION

In 2009, the Next Generation Safeguards Initiative (NGSI) of the U.S. Department of Energys National Nuclear Security Administration (NNSA) began a five-year effort to develop an integrated instrument fully capable of determining Pu mass in, and detecting diversion of pins from, spent commercial fuel assemblies[1]. Following a rigorous, MCNPX-based[2] evaluation of 14 individual measurement techniques against a library of 64 spent fuel assemblies, efforts in 2012 will turn to the construction of one or more integrated systems comprised of the most promising techniques. This project brings together measurement and modeling experts from multiple U.S. national laboratories, several universities, and potentially one or more international partners.

Nuclear resonance fluorescence (NRF) has been studied as one of the 14 measurement techniques . NRF is a well-known physics phenomenon in which a nucleus absorbs an incident photon and is excited to a resonant state. Such states are generally very short-lived and subsequently de-excite by emission of one or more γ rays. Both the energies of the NRF γ rays and the energies at which resonant absorption occur are isotope-specific. Therefore, observed rates of these processes can be used to quantify the isotopic content within an irradiated target[3, 4]. A key advantage of NRF is that the measured signatures directly relate to the concentration of the isotope and an unfolding of combined responses from several fissile isotopes is not required. Because of this, NRF is significantly less subject to systematic uncertainties resulting from measurements.

As part of the NGSI effort, analytical modeling and Monte Carlo simulations using MCNPX were performed to determine the system requirements for quantitatively measuring ^{235}U and ^{239}Pu in spent nuclear fuel using NRF.

II. PERFORMING NRF MEASUREMENTS

Techniques used to perform NRF measurements involve a photon source that excites resonances and a measurement system that either directly measures NRF γ-ray emissions or a downstream system that measures the reduced spectral intensity of photons that have been resonantly absorbed. The two types are referred to as backscatter and transmission measurements, respectively. Both backscatter and transmission measurements can be made using photon sources with very large energy spreads, such as bremsstrahlung sources. However, quasi-monoenergetic (QM) photon sources, the subject of more recent development, have been proposed for NRF measurements[5–8].

An example backscatter NRF measurement geometry is schematically shown in Figure 1(a). Photons emitted from a bremsstrahlung converter are collimated towards a target fuel assembly. Arrays of γ-ray detectors positioned at large angles, relative to the incident photon beam, measure photons scattered from the assembly. A significant challenge for performing backscatter NRF measurements on spent nuclear fuel is the intense radiation emitted from fission products. A combination of detector collimation (not indicated in Figure 1(a)) and γ-ray filters, i.e. thick attenuators placed directly between the assembly and the γ-ray detectors, must be used to reduce the radioactive background. Likewise, filter design, detector characteristics, and photon beam parameters such as energy distribution, temporal profile, and overall beam intensity were treated as adjustable parameters in our study.

An example transmission measurement configuration is shown in Figure 1(b). It is described in more detail in Ludewigt et al.[9]. In the transmission geometry, the source photon beam transmitted through the target assembly is intercepted by a *transmission detector foil*, which is a sheet comprised of a nearly pure isotope. Detectors are positioned to measure the photons scattering in the foil. The reduction in rate at which the detectors measure NRF occurring in the transmission detector foil isotope is indicative of the areal density of the same isotope in the fuel assembly. In this geometry, the γ-ray detectors are well-shielded from the radioactivity of the spent fuel. Parameters that may be adjusted in this geometry include all those mentioned for the backscatter geometry, as well as the thickness of the transmission detector.

Measured NRF responses of ^{235}U, ^{236}U, ^{238}U, ^{237}Np and weapons-grade Pu (93% ^{239}Pu) can be found in the literature[3, 10–14]. Recently, NRF spectra of ^{240}Pu have also been measured[15]. ^{235}U shows moderately weak NRF resonances between 1.6 and 1.9 MeV, ^{239}Pu appears to have weaker resonances between 2.1 and 2.5 MeV, and the even isotopes, ^{236}U, ^{232}Th and ^{238}U have demonstrated stronger, but non-overlapping resonances between 2 and 2.5 MeV. ^{238}U has also been observed to undergo weaker NRF transitions in the ^{235}U NRF energy range. Several strong ^{240}Pu resonances were observed between 2.2 and 2.8 MeV. Actinide resonance energies tend to be below thresholds for most particle-emission reactions. Therefore, the primary interaction methods are photo-atomic scattering such as incoherent scatter and pair production. Incoherent scatter primarily results in forward-scattered photons although large-angle, lower-energy scattered photons are also produced. Pair production results in the isotropic emission of two 511 keV annihilation photons. These two processes produce the majority of the background due to interrogating photons.

Spent fuel compositions used to describe radioactive emission rates and Pu content were calculated using the computer code, OrigenARP 5.1.01 (referred to herein as Origen) that is distributed with the Scale 6 software package[16].

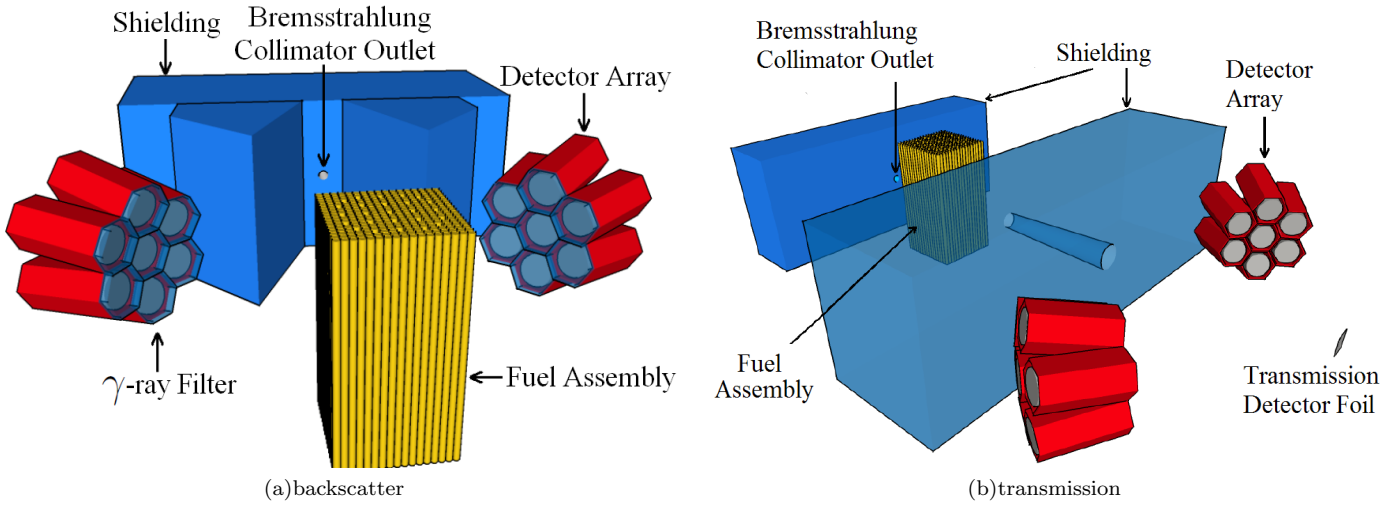

FIG. 1. Schematic NRF measurement geometries.

These calculations indicate that the mass of ^{239}Pu in a 17x17 PWR fuel assembly with 45 GWd/MTU burnup is ~2.4 kg. This corresponds to an average ^{239}Pu areal density for a horizontal cut-through of an assembly of 0.25 to 0.4 g/cm^2, depending on the rotation of the fuel assembly. The maximum ^{239}Pu areal density, along a line through the center of a row of fuel pins is 0.72 g/cm^2.

For both geometries, the accrual of sufficient statistics is the main challenge associated with precise measurements of Pu concentrations. The statistical uncertainty trends with the square root of measurement duration for a given geometry. We therefore arbitrarily assume a desired measurement precision, such as 3% and determine the necessary number of NRF counts that would result in a statistical uncertainty equal to the assumed precision noting that the number of counts needed for a different precision is easily scaled. For a single NRF resonance in the backscatter geometry, the fractional statistical uncertainty of an isotopic concentration in the assay target, $\frac{\sigma_N}{N}$, associated with C_{NRF} counts in a sufficiently isolated photo-peak is given by:

$$\frac{\sigma_N}{N} = \sqrt{\frac{1+2/\xi}{C_{\mathrm{NRF}}}} \tag{1}$$

where ξ is the signal-to-background ratio of the measured NRF peak. Similarly, the statistical uncertainty in areal density associated with a transmission measurement is given by

$$\frac{\sigma_{Nx}}{Nx} = \frac{1}{\alpha Nx}\sqrt{\frac{1+2/\xi}{C_{\mathrm{NRF}}}} \tag{2}$$

where α is the coefficient that relates the measured rate of attenuation in the assembly of resonant-energy photons due to NRF to areal density, Nx, of the resonant isotope in the assembly. The quantity, α, is obtained by evaluating the absolute value of the derivative of the *effective attenuation* curve (Figure 2) for a particular resonance at the corresponding areal density. The derivation of effective attenuation, i.e. the reduced rate at which NRF occurs in the detector foil occurs due to resonant attenuation in the target is given in Quiter et al.[3]. Example effective attenuation curves are shown for ^{239}Pu resonances (based on measurements described in Bertozzi et al.[10], assuming that the integrated resonance strength is the sum of the strength for the 2143.5 and 2135 keV lines tabulated) and for a stronger ^{238}U resonances [3, 12] in Figure 2. Clearly, the larger ^{238}U resonance results in a steeper effective attenuation curve and a larger value of α. This implies that statistical uncertainties in transmission measurements are proportional to the inverse of the resonance strength to the power of 1.5-2.

III. BACKSCATTER SYSTEMS

System requirements for backscatter NRF measurement systems were studied using the following method: the photon flux at a hypothetical detector position due to radioactive emissions from spent fuel was estimated using Origen

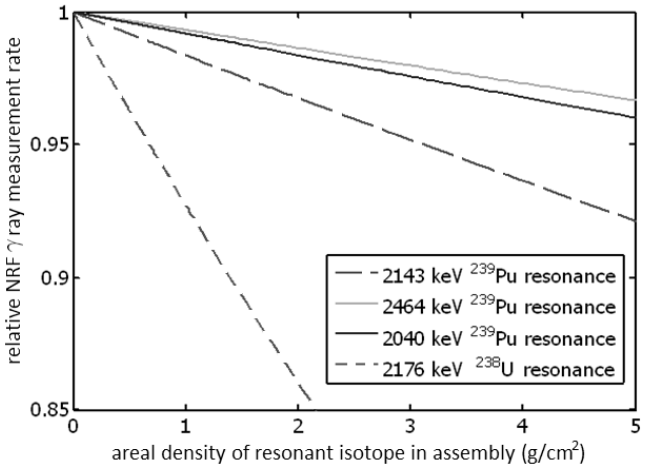

FIG. 2. Selected effective attenuation curves for ^{239}Pu and ^{238}U resonances.

and MCNPX; the photon flux at the hypothetical detector position due to scatter of resonant-energy interrogating photons incident upon the assay target was calculated using MCNPX; the photon flux at the hypothetical detector position due to scatter of nonresonant-energy interrogating photons incident upon the assay target was calculated; and the photon fluxes were combined by simulating filter and radiation detector responses and considering limitations such as input count-rates and energy resolution. The base-line detector response is taken to be a conservative performance estimate of a 100% relative efficiency high-purity Ge (HPGe) detector that has 3 keV full-width at half-maximum resolution at 2.5 MeV and operates at a maximum rate of 20 kHz without spectral degradation. Significantly faster HPGe performance has been reported[17], and increased count rates would typically proportionally improve estimated measurement times. When the use of a higher rate detector type that sacrafice resolution could benefit the application, it is mentioned in the text.

The first step involved performing Origen calculations to determine the photon emission rate from the radioactive spent fuel. This included γ-ray emissions due to radioactive decay, bremsstrahlung from emitted β particles, and prompt fission γ ray emissions. Example spectra are shown as photon fluxes at 1 m from the center of 40 GWd/MTU burn-up PWR fuel assembly with cooling times of 5-20 y in Figure 3(a) for an uncollimated geometry. Above the well-know Cs lines, the spectrum has a strong line at 1596 keV due to ^{154}Eu, which has a 8.5 y half-life. Below this energy, measurement of NRF peaks would be very difficult due to the intense radioactive background. However above 1600 keV, there are still numerous energetic photons emitted. The majority of these are γ rays due to ^{144}Pr and ^{106}Ru, which are short-lived daughters of parents that have approximately 1 y half-lives. Energetic photons may also be produced by bremsstrahlung emission from the β particles emitted by ^{144}Pr and ^{106}Ru and from fission γ rays resulting from spontaneous and neutron-induced fission of the actinides. These energetic photons are less commonly examined in passive spent fuel spectroscopy because they are less intense and the detectors used in such experiments are often small, which significantly reduces the likelihood of full-energy depositions. However, the photons do provide a non-negligible background in NRF counting experiments.

The Origen-calculated photon emission rate for the 11 y cooled PWR fuel was used as a source term for subsequent MCNPX simulations. In the MCNPX simulations, a 100% relative efficiency HPGe detector was collimated to view one linear centimeter of one fuel pin within the irradiated assembly and was placed behind a Pb filter whose thickness was varied from 5-10 cm. Again, the detector was positioned 1 m from the center of the assembly. Due to the geometry of fuel assemblies, such collimation geometry must unavoidably accept radioactive emissions from fuel pins in other rows of the assembly, as well as from the intended fuel pin. In this collimation geometry, counting spectra such as those shown in Figure 3(b) result, although the energy bins are 25 keV wide - obscuring peaks that would otherwise be visible. The overall count rates, determined by integrating these spectra for 5.0, 7.5 and 10 cm thick Pb filters are 1.7×10^5, 2.2×10^4, and 3.8×10^3 counts/s, respectively. This indicates that for this geometry, very high count rate detectors or thick filters must be be used, or that measurements must be made on fuel that has cooled for longer than a decade. Alternatively, the detection geometry could be modified to reduce the effective solid angle of the collimated detector subtended by the fuel. However decreasing the viewing window of the detector would proportionally decrease NRF count rates, which would further increase measurement durations for a given number of γ-ray detectors.

Having considered radioactive emissions, we now examine expected count rates due to interrogating photons. We first assume that source photon collimation is sufficient such that source photons are not incident upon radiation detectors unless they scatter within the irradiated assembly. Photons that do interact in the fuel assembly may

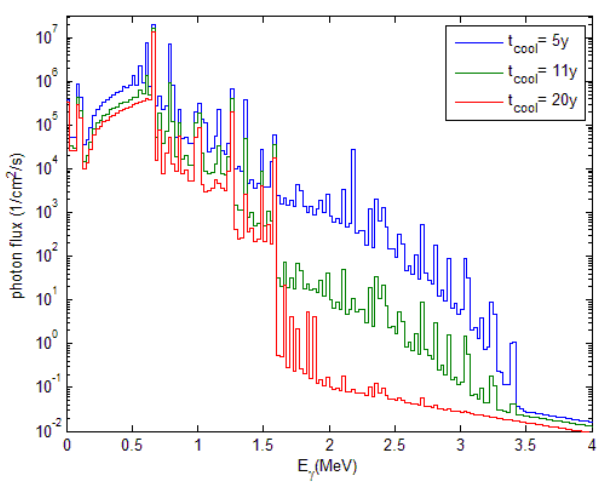

(a)Photon flux for cooling times of 5, 11, and 20 y . Energy bins are 25 keV wide.

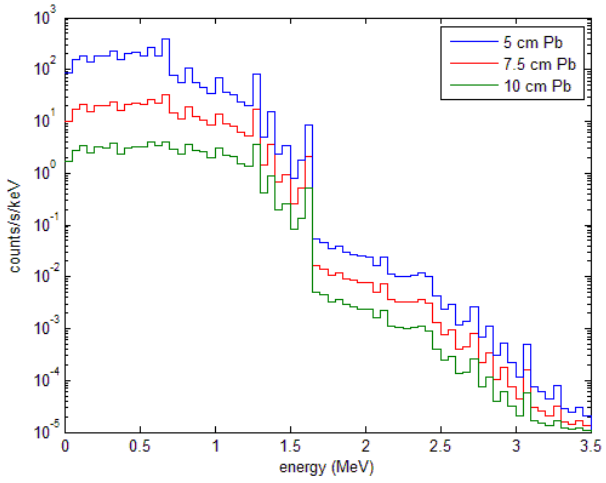

(b)Energy depositions in collimated 100% HPGe detector behind 5, 7.5 and 10 cm of Pb.

FIG. 3. Calculated spectra due to spent fuel radioactivity at 100 cm from the center of a 17x17 PWR fuel assembly that has undergone 45 GWd/MTU burn-up.

undergo NRF, elastic scatter, or a variety of inelastic scatter processes. NRF has been added to MCNPX[18–20] and the code's elastic photon scatter routines have been improved[21]. It is assumed that the code accurately simulates incoherent scatter and bremsstrahlung produced by photo-electrons[22]. As a result, MCNPX is used to determine photon intensities and count rates due to NRF and non-resonant scattering at the detector positions.

Example backscatter spectra due to a 2.432 MeV photon beam with an 8 eV energy width are shown in Figure 4(a)[1]. In these simulations, the photons are either tuned to the ^{239}Pu resonance or to a nearby, but non-resonant energy[2]. The interrogating photons are assumed to be normally incident upon a fuel assembly that contains 0.4% by weight ^{239}Pu and are collimated such that only a single row is irradiated and only one irradiated pin is viewed as is shown in Figure 4(b).

The spectra appear nearly identical, except near the energy of the source photon, where NRF increases the height of the elastic scatter peak and also produces another peak due to de-excitation of the NRF level to a low-lying excited state in ^{239}Pu. While the visibility of the NRF photons in the simulated spectrum may appear encouraging, there are important factors that make NRF measurements very difficult. The first is that even for an 8 eV-wide source centered on the NRF resonance, induced NRF γ rays contribute approximately one thousandth of the total photon flux seen an unfiltered detector. Similarly, the intensity of NRF photons in the source photon energy bin is only 7 times that due to non-resonant elastic scatter ($\xi_{max} \approx 7$). Also, the intensity of NRF photons is quite low - 3.1×10^{-10}/cm^2/source photon - indicating that 1.6×10^{-8} NRF photons per source photon would reach a detector with a 50 cm^2 effective area, positioned 1 m from the irradiated pin. To achieve 3% statistical uncertainty, a minimum of 1,400 counts would be necessary. With an ideal detector that measures the full energy of all incident photons, approximately 9×10^{10} source photons within the 8 eV energy band would need to be directed towards the fuel pin. In practice, γ-ray detectors cannot measure full-energy depositions with 100% efficiency and are rate-limited. Therefore, spent fuel activity cannot be neglected, resulting in lower values of ξ. Furthermore, real photon sources have demonstrated bandwidths that are significantly wider, several keV wide for QM sources, or an exponential spectrum for bremsstrahlung-based sources, resulting in increased overall count rate burdens of γ-ray detectors and a worse signal to-background-ratio depending on the γ-ray detector resolution.

The Origen/MCNPX calculations indicate that the flux due to photon emissions from 11 y-cooled spent fuel in the assumed geometry is approximately 3 photons/cm^2/s. In order for the intensity due to ^{239}Pu resonance excitation to be equal to the radioactive flux, a QM photon source would need to produce 10^9 photons/eV/s, incident upon the assembly within the dimensions of 1 linear cm of a fuel pin.

In this paper we consider several examples using quasi-monoenergetic (QM) photon sources whose energy profile is

[1] The 8 eV bandwidth was selected to encompass the entirety of the resonances as defined in MCNPX.
[2] Recent measurements indicate that this resonance, which was attributed to ^{239}Pu [10], may actually be due to ^{240}Pu.

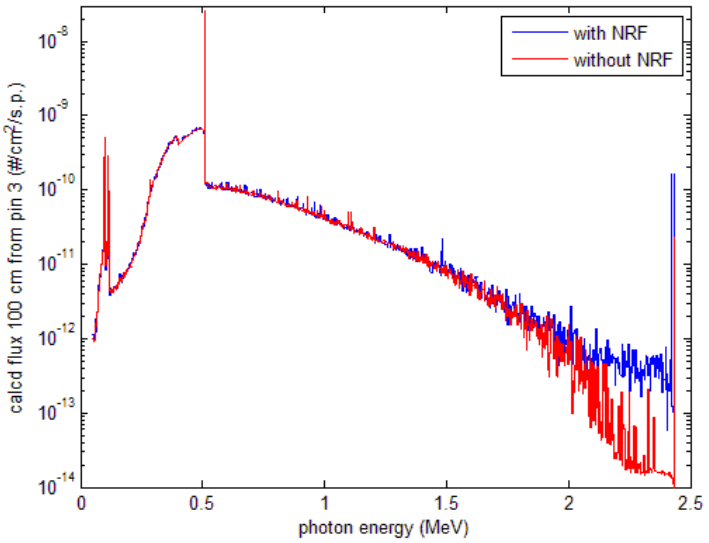

(a)MCNPX-computed spectra due to backscatter of monoenergetic photons at resonant (blue) and a nearby non-resonant energy (red) incident upon a single row of a spent fuel assembly. See text for description of the simulated geometry.

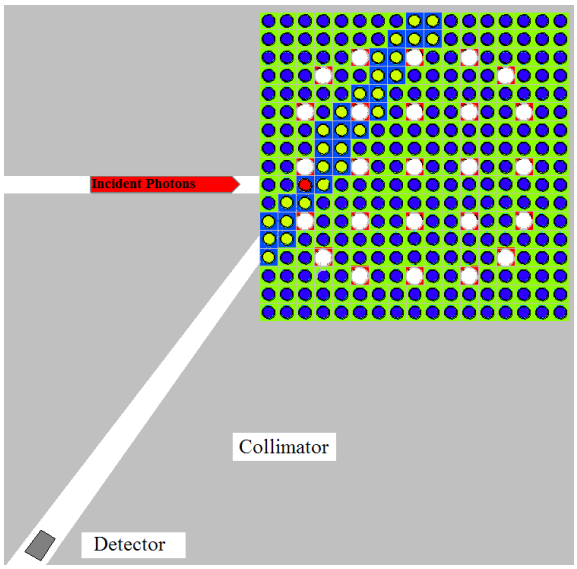

(b)Simulated collimation geometry for example calculations of backscatter NRF measurements and radioactive emissions.

FIG. 4.

TABLE I. Influence of QM photon sources with bandwidths larger than the detector resolution. Although not indicated, ξ will not significantly change after σ_S becomes larger than detector resolution.

σ_S (keV)	#res/#non-res	ξ
0.02	1.9×10^{-1}	1.1
0.1	3.3×10^{-2}	2.2×10^{-1}
1.0	3.2×10^{-3}	2.2×10^{-2}
3.0	1.1×10^{-3}	7.5×10^{-3}
10.	3.2×10^{-4}	2.2×10^{-3}
100.	3.2×10^{-5}	2.2×10^{-4}

assumed to be described by a Gaussian distribution with width σ_S:

$$P(E) = \frac{1}{\sqrt{2\pi\sigma_S^2}} \exp\left[\frac{-(E - 2432\text{keV})^2}{2\sigma_S^2}\right] \tag{3}$$

By integrating Equation 3 over an energy range of ±4 eV, for various values of σ_S, we can determine the fraction of QM source photons that would produce the backscattered flux due to resonant-energy source photons (blue in Figure 4(a)), compared to the remainder of the source spectrum that only produces the non-resonant backscattered flux (red in Figure 4(a)). That relatively few of the source photons are resonant in energy results in two problems for backscatter NRF measurements. First, the signal-to-background, ξ, ratio of an NRF peak is significantly reduced by the elastic backscatter of non-resonant source photons, resulting in the values shown in Table I, until $\sigma_S \sim \xi$. Once $\sigma_S > \xi$, the bandwidth of the source beam does not strongly effect ξ, i.e., systems with $\sigma_S > 3$ keV that have 3 keV resolution detectors will have a $\xi \approx 7.5 \times 10^{-3}$. Such a low signal-to-background ratio indicates that ≈ 210 times as many NRF counts are necessary to achieve the same statistics as in the ideal, ξ_{max} case (from Equation 1).

The second effect of QM photon source bandwidth is the increase in overall detector count rates with increasing bandwidth. For slower detectors such as HPGe, this is problematic. For example, in order for the 3 keV-wide beam to produce 3% uncertainty, we estimate from Equation 1 that 3×10^5 NRF counts are necessary. Assuming 20% full energy deposition within the detector and a single 50 cm^2 surface area 1 m from the assembly, this would require at least 10^{14} resonant energy source photons, corresponding to 10^{17} total source photons incident upon the fuel assembly, which would induce a total of 3×10^{11} total counts in the detector, unless a filter were used. Assuming a HPGe detector operating at 20 kHz, this implies 1 NRF count every minute in the detector and a limit to the QM source strength

TABLE II. Measurement durations in units of 'number of 100% relative efficiency HPGe detectors·time' necessary to obtain stated statistical uncertainty in ^{239}Pu concentrations in a single fuel pin located in the 3rd row of an assembly, using 2.6 MeV endpoint energy bremsstrahlung.

I_e (mA)	t_{meas} (det·yr)	FOM
0.01	5.0×10^{7}	0.03
0.10	5.0×10^{5}	0.11
1.0	610	0.31
10	13.3	0.65
45	1.7	0.86
100	1.5	0.93

of 5×10^{9} photons/s. Adding a filter significantly reduces the low-energy count rate and reduces the NRF-energy count rate less, due to less attenuation of more-energetic photons. With a 7.5 cm filter, the maximum source strength allowed by the 20 kHz detector count rate limit increases to 3×10^{12} photons/s, and the total measurement time drops by a factor of approximately 14.

Whereas detector count rate limitations are problematic for backscatter NRF measurements using QM photon source, they are nearly prohibitive if bremsstrahlung is used as the photon source. Measurement durations necessary to obtain 3% uncertainties, in units of the product of number of 100% relative efficiency HPGe detectors and time are tabulated in Table II for several beam intensities, assuming a 2.6 MeV endpoint energy bremsstrahlung spectrum. The value labeled 'FOM' in the fourth column indicates the 'figure of merit' for a measurement with the stated beam current. A FOM of unity indicates that NRF counting statistics accrue at the same rate as they would if there were no spent fuel radioactivity. The stronger the current, the less significant is the radioactive background. For beam currents below 50 mA, a 7.5 cm Pb filter was assumed. At 100 mA, the large beam-induced flux requires a 10 cm thick Pb filter to keep total count rates below 20 kHz. Because of this, estimated measurement times, which had rapidly decreased with increasing beam current, begin to plateau[3].

Systems using pulsed photon sources can reduce the effect of radioactive backgrounds by ignoring detected events that do not arrive during the source pulse interval. Therefore they may be able to achieve FOM values according to their 'beam-on' average current rather than the 'pulse cycle' average current. However, unless pulsed sources are capable of very high duty factors, the time lost while not counting outweighs the benefit of improved FOM values, making pulsed sources generally slower than a comparable continuous source.

IV. TRANSMISSION SYSTEMS

Similar to the study of backscatter systems, it was also assumed that detector count rate limitations constrain transmission NRF measurement systems. Signal-to-background ratios for the measurement of NRF peaks can be significantly improved by the use of nearly isotopically pure detector foils, but since the Pu content in the assembly is indicated by the reduction in NRF γ-ray intensities, statistical precision of transmission measurements do not correspondingly improve. Also, the ability to shield the photon detectors from the radioactive emissions from the fuel assembly basically eliminates issues associated with spent fuel radioactivity. However, small NRF cross sections produce small values of α (in Equation 2) for resonances of interest and cause difficulties in obtaining good measurement statistics.

A bremsstrahlung beam has the advantage that it can excite multiple resonances at the same time, however it also produces large amounts of non-resonant photons that contribute to detector count rate burden. Using a 2.8 MeV endpoint energy bremsstrahlung beam incident upon a fuel assembly we determine the photon flux spectrum at an assumed detector location, 1 m from a 1 cm thick ^{239}Pu transmission detection foil. The flux is normalized to the charge deposited in the bremsstrahlung converter by the electron beam. The converter is positioned 2.4 m from the transmission detection foil. The assembly is rotated 30° to minimize streaming paths through the assembly, resulting in an average ^{239}Pu areal density of 0.4 g/cm^2. The resulting calculated spectrum is shown in Figure 5 and the insert highlights the calculated NRF energy region (with 3 keV-wide energy bins). Using this calculated spectrum and an

[3] This would not be the case for faster detector systems

TABLE III. Maximum bremsstrahlung-producing electron currents, I_{max}, for 2.8 MeV electrons and various filter thicknesses in the studied transmission geometry, assuming a maximum count rate of 20 kHz and a 50 cm^2 surface area detector.

x_f (cm)	I_{max} (mA)
1.27	2.5
2.54	11
5	96
7.5	510

assumed detector response, we determine the maximum beam intensity, I_{max}, allowable for a given filter thickness assuming an acceptable count rates 20 kHz. These values are shown in Table III.

Assuming a 5 cm thick filter and a 96 mA beam, possibly produced by a Rhodotron[23] or similar device, the NRF count rate, C_{NRF}, and ξ are determined for each NRF energy. Using theoretically derived values for α, we use Equation 2 to predict the statistical uncertainty, $\sigma(E)$, associated with the attenuation measurement for each NRF resonance. Assuming the areal densities determined by each resonance are combined by a weighted mean with $w_E = 1/\sigma_E^2$, the statistical error associated with the averaged areal density measurement is calculated. By scaling the measurement time, which proportionally scales the integrated electron charge incident upon the bremsstrahlung converter, we may determine the measurement duration necessary for a given precision measurement for the geometry. These values are tabulated in Table IV along with resonance information, expected signal-to-background ratios (assuming 3 keV FWHM detector resolution), and expected count rates. It should also be noted that the non-resonant elastic scatter of NRF photons remains inaccurate and under-predicted in MCNPX[24] and therefore values of ξ reported in the table remain somewhat inaccurate.

In order to reach the statistical uncertainties for each line shown in Table IV, one would need the product of integrated current and number of 100% relative efficiency HPGe detectors to be $8{\times}10^6$ Coulombs. Assuming 96 mA beam, this implies a one day measurement could be accomplished if 1040 detectors were positioned at a distance of 1 m from the transmission detector foil. This would be possible, although not practical, as a 1 m radius hemisphere could accomodate ∼1,260 such detectors. Also, faster detectors could reduce measurement times or the required number of detectors.

QM photon sources potentially reduce filter requirements and may allow intense interrogating beams tuned to a single resonance. For consideration of QM sources, MCNPX was used to calculate photon fluxes at a detector position due both to resonant energy and non-resonant energy photons incident upon a transmission system. NRF count rates, signal-to-background ratios, and total count rates were then estimated for a variety of bandwidths. Using the 2432 keV ^{239}Pu resonance, and assuming that the 2423 keV NRF γ ray is due to de-excitation of the 2432 keV ^{239}Pu resonance, we obtain $\alpha = 0.016$ cm^2/g for transmission through the center of a row of fuel pins. Using this for α and estimated values of ξ, assuming HPGe detector resolution, Equation 2 was used to determine the necessary number of NRF counts that would provide 3% statistical uncertainty in a ^{239}Pu measurement in a fuel assembly, with $N_{^{239}\mathrm{Pu}}x = 0.72$ g/cm^2. These numbers, shown in Table V, are translated to a minimum measurement time (in units of the product of measurement duration in days and the number of 100% relative efficiency HPGe detectors), are listed in the table,

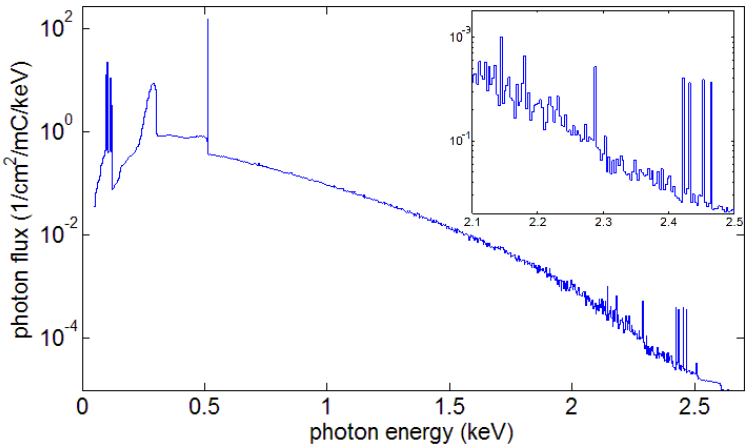

FIG. 5. Calculated photon flux spectrum emitted from a detection foil towards a detector. The inset highlights the NRF energy region.

TABLE IV. Bremsstrahlung source transmission measurement parameters necessary to perform a 3% measurement of ^{239}Pu in a spent fuel assembly where $N_{239_{\rm Pu}}x = 0.40$ g/cm^2, assuming HPGe detectors operate at 20 kHz and a 5 cm Pb filter is used. The asterixes indicate that the pair of γ ray energies are assumed to be due to different de-excitation modes of a single resonance.

E_{res} (keV)	$\int \sigma_{\rm NRF} dE$ (ev·b)	α (cm^2/μg)	ξ	NRF counts (1/detector · C)	$\sigma_{N_{239\,Pu}x}$ (%)
2047	5	8.1	0.03	0.10	260
2135*	4	16.4	0.14	0.24	41
2144*	13	16.4	2.2	2.2	4.7
2289	8	7.2	1.0	1.0	16.0
2423*	10	16	10.2	0.99	5.9
2432*	9	16	8.7	0.83	6.5
2454	9	7.7	9.5	0.92	12.7
2465	8	6.8	11.7	1.0	13.7
total				7.3	3.0

TABLE V. Transmission measurement parameters necessary to perform 3% measurment of ^{239}Pu in spent fuel assembly where $\rho_{\rm Pu} = 0.72$ g/cm^2, assuming HPGe detectors operate at 2×10^4 Hz.

σ_S (keV)	$\Phi_{\rm NRF}^{\sigma_S}$ (1/cm^2/ph)	$\Phi_{\rm T}^{\sigma_S}$ (1/cm^2/ph)	ξ	NRF counts	t_{meas} (det·day)	intensity (1/eV/s)
0.1	3.1×10^{-11}	3.3×10^{-9}	22	9.1×10^{6}	2.8	4.0×10^{8}
0.3	1.1×10^{-11}	3.3×10^{-9}	7.5	1.1×10^{7}	10	1.3×10^{8}
1	3.1×10^{-12}	3.3×10^{-9}	2.6	1.5×10^{7}	45	4.0×10^{7}
2	1.6×10^{-12}	3.3×10^{-9}	2.1	1.7×10^{7}	100	2.0×10^{7}
3	1.1×10^{-12}	3.3×10^{-9}	2.0	1.7×10^{7}	160	1.3×10^{7}
5	6.3×10^{-13}	3.3×10^{-9}	1.9	1.7×10^{7}	270	8.1×10^{6}
10	3.1×10^{-13}	3.3×10^{-9}	1.9	1.7×10^{7}	520	4.0×10^{6}
20	1.6×10^{-13}	3.3×10^{-9}	1.9	1.7×10^{7}	10^3	2.0×10^{6}

assuming a 20 kHz count rate. Lastly, the necessary peak intensity of a QM beam that would produce a total 20 kHz count rate in a HPGe detector is also shown. The values all assume that no filter is used. Filters could be used to allow broader bandwidth source beams to operate at higher intensities than those shown in the table, but the rate at which NRF counts were measured would also be reduced, although less so than the lower-energy portion of the spectrum.

Lastly, if very narrow bandwidth, several keV width or less, sources are used, high-rate detectors such as scintillation detectors, capable of operating at MHz rates could greatly improve the performance of a transmission NRF system. Systems with several large γ-ray detectors, could conceivably achieve few percent statistical uncertainties from measurement durations on the order of an hour.

V. CONCLUSIONS AND OUTLOOK

The precise determination of Pu or minor actinide content in spent nuclear fuel assemblies is challenging due to low NRF signal rates and the relatively intense non-resonant scattered background. For backscatter NRF measurements the background is further increased by radioactive emissions from the spent fuel and significant improvements in beam intensity, beam energy spread, detector resolution and count rate capability are needed. Even with technology that is currently in the proposal state, backscatter measurements would require large detector arrays and unrealistically long counting times in order determine Pu content to a precision of a few percent.

For transmission measurements the outlook is more favorable. Our modeling results indicate that a system could be built that would measure the areal density of the most abundant Pu isotopes (239, 240) in spent fuel with a percent-level uncertainty. For a system based on a bremsstrahlung beam the large associated detector array would be costly and technically challenging[25] and measurement times would still be quite long. Potentially much higher

performance could be achieved with near mono-energetic photon sources based on laser Compton scattering. However, the technology must be further developed to provide the high beam intensities and small energy spreads needed for low uncertainty measurements. Furthermore, such measurements will require more precise actinide NRF cross-section data.

In future advanced nuclear fuel cycles, minor actinides will become increasingly abundant, and new methods to determine their concentrations and the fissile content in fuel will be needed because current non-destructive analysis methods rely on measuring correlated quantities that are convolutions of signals from all fissile isotopes. Such methods become increasingly prone to serious systematic errors with the presence of more transuranic isotopes. NRF, in contrast, is isotope-specific and allows the measurement of an isotopic concentration independently of other isotopes present in the fuel.

Lastly, it should be acknowledged that, although NRF measurement systems require further advances in source and/or detector technologies and will likely be costly, they could potentially provide currently unattainable safeguards capabilities, i.e., determining the amount of a specific fissile isotope and pin diversion in spent fuel. Furthermore, their total cost would likely represent a small fraction of the total cost of a newly-constructed fuel reprocessing facility.

ACKNOWLEDGMENTS

This work was supported by the Offices of Proliferation Detection and Nonproliferation & International Security of the National Nuclear Security Administration, US Department of Energy under Contract No. DE-AC02-05CH11231.

[1] K.D. Veal, S.A. LaMontagne, S.J. Tobin, L.E. Smith, NGSI Program to Investigate Techniques for the Direct Measurement of Plutonium in Spent LWR Fuels by Non-destructive Assay, Institute of Nuclear Materials Management 51st Annual Meeting, Baltimore, MD (July 11-16, 2010).

[2] J.F. Pelowitz (ed.), "MCNPX^{TM} USERS MANUAL Version 2.6.0," LA-CP-07-1473 (2008).

[3] B.J. Quiter, B.A. Ludewigt, V.V. Mozin, C. Wilson, and S. Korbly, "Transmission Nuclear Resonance Fluorescence Measurement of ^{238}U," Nucl. Inst. Meth. Phys. Res. B 269 (2011) pp. 1130-1139.

[4] W. Bertozzi and R.J. Ledoux, "Nuclear resonance fluorescence imaging in non-intrusive cargo inspection," Nucl. Instr. Meth. Phys. Res. B 241 (2005) pp. 820-825.

[5] C.G.R. Geddes, E. Cormier-Michel, E.H. Esarey, C.B. Schroeder, J-L. Vay, W.P. Leemans, and the LOASIS team, LBNL; D.L. Bruhwiler, J.R. Cary, B. Cowan, M. Durant, P. Hamill, P. Messmer, P. Mullowney, C. Nieter, K. Paul, S. Shasharina, S. Veitzer, and the VORPAL development team, Tech-X; G. Weber, O. Rubel, D. Ushizima, Prabhat, and E.W. Bethel, VACET; and J. Wu, SciDAC Scientific Data Management Center, "Laser Plasma Particle Accelerators: Large Fields for Smaller Facility Sources," SciDAC Review 13, pp. 13 (2009). LBNL-2299E.

[6] T. Hayakawa, N. Kikuzawa, R. Hajima, T. Shizuma, N. Nichimori, M. Fujiwara, and M. Seya, "Nondestructive assay of plutonium and minor actinide in spent fuel using nuclear resonance fluorescence with laser Compton scattering γ-rays," Nucl. Inst. Meth. Phys. Res. A 621 (2010), pp. 695-700.

[7] C.A. Hagmann, J.M. Hall, M.S. Johnson, D.P. McNabb, J.H. Kelley, C. Huibregtse, E. Kwan, G. Rusev, and A.P. Tonchev, "Transmission-based detection of nuclides with nuclear resonance fluorescence using a quasimonoenergetic photon source," J. of App. Phys. 106, (2009) 084901.

[8] E. Bulyak, P. Gladkikh, T. Omori, V. Skomorokhov, and J. Urakawa, "Compton ring for nuclear waste management," Nucl. Inst. Meth Phys. Res. A 621 (2010), pp. 105-110.

[9] B.A. Ludewigt, V.V. Mozin, A.H. Haefner and B.J. Quiter, "Using Nuclear Resonance Fluorscence for Nondestructive Isotopic Analysis," Inst. of Nucl. Mat. Man., 51st Ann. Mtg., Baltimore, MD, July 11-15 (2010).

[10] W. Bertozzi, J.A. Caggiano, W.K. Hensley, M.S. Johnson, S.E. Korbly, R.J. Ledoux, D.P. McNabb, E.B. Norman, W.H. Park, and G.A. Warren, "Nuclear resonance fluorescence excitations near 2 MeV in ^{235}U and ^{239}Pu," Phys. Rev. C 041601(R) (2008).

[11] J. Margraf et al., "Photoexcitation of low-lying dipole transitions in ^{236}U," Phys. Rev. C 42 (1990), pp. 771-774.

[12] R.D. Heil, H.H. Pitz, U.E.P Berg, U. Kneissl, K.D. Hummel, G. Kilgus, D. Bohle, A. Richter, C. Wesselborg, and P. Von Brentano, "Observation of orbital magnetic dipole strength in the actinide nuclei ^{232}Th and ^{238}U." Nuc. Phys. A476 (1988), pp. 39-47

[13] A. Zilges, P. von Brentano, R.-D. Herzberg, U. Kneissl, J. Margraf, H. Maser, N. Pietralla, and H.H. Pitz, "Strong dipole excitations around 1.8 MeV in ^{238}U," Phys. Rev. C 52 (1995), pp. R468-R470.

[14] C. Angell et al., "Nuclear resonance fluorescence of ^{237}Np," Phys. Rev. C 82 054310 (2010).

[15] The authors of this paper and Passport Systems Inc. collaborated in these measurements. The results have not yet been published.

[16] SCALE-4.3, Modular System for Performing Standardized Computer Analyses for Licencing Evaluation. Oak Ridge National Laboratory, 1997. RSICC Computer Code Collection CCC-0545/12.

[17] J. Plagnard, J. Morel, A. Tran Tuan, "Metrological characterization of the ADONIS system used in gamma-ray spectrometry," App. Rad. and Isot. 60 (2004) 179-183.
[18] B.J. Quiter, B.A. Ludewigt, V.V. Mozin, S.J. Tobin, "Nondestructive Spent Fuel Assay Using Nuclear Resonance Fluorescence," *Annual Meeting of the Institute of Nuclear Material Management*, Tucson, AZ, 2009.
[19] Gregg W. McKinney, Alex B. McKinney, John S. Hendricks, Denise B. Pelowitz, and Brian J. Quiter, "MCNPX NRF LIBRARY - RELEASE 2," *ANS Annual Meeting*, San Diego, CA, June 2010.
[20] M.R. James, G.W. McKinney, J.W. Durkee, M.L. Fensin, J.S. Hendricks, D.B. Pelowitz, R.C. Johns, L.S. Waters, J.S. Elson, M.W. Johnson, B. Quiter, "Implementation of Homeland Security Features in MCNP/X," *IEEE NSS*, Oct. 31-Nov. 6, 2010, Knoxville, TN, LA-UR-10-07256.
[21] John S. Hendricks and Brian J. Quiter, "MCNP/X Form Factor Upgrade for Improved Photon Transport," (LA-UR-10-01096) *Journal of Nuclear Technology*, p. 150, Vol. 175, July 2011.
[22] C. Hagmann and J. Pruet, "Photon production through multi-step processes important in nuclear resonance fluorescence experiments," Nucl. Instr. Meth. Phys. Res. B 259 (2007) pp. 895-908.
[23] J. Pottier, "A new type of RF electron accelerator: the rhodotron," Nucl. Instr. Meth. Phys. Res. B 40/41 (1989) pp. 943-945.
[24] S.D. Ambers, B.J. Quiter and B.A. Ludewigt, "Importance of Elastic, Non-Resonant Scattering in the Assessment of NRF for NDA," *52nd Annual INMM Meeting*, July 17-21, 2011, Palm Desert, CA.
[25] I-Yang Lee, "GRETA White Paper for the 2007 NSAC Long-range Plan," available online at `http://grfs1.lbl.gov/`
[26] S.J. Tobin et al., "Determining Plutonium in Spent Fuel with Nondestructive Assay Techniques," Proc. of 31st Ann. Mtg. of ESARDA, Vilnius, Lithuania (2009).
[27] F.R. Metzger, "Resonance Fluorescence in Nuclei," Prog. in Nuc. Phys. 7, (1959) pp. 54.